Gapless surface electronic structure of $1T$-$TiSe_2$ in the distorted phase

Turgut Yilmaz* and Elio Vescovo
National Synchrotron Light Source II, Brookhaven National Lab, Upton, New York 11973, USA

(Received 17 July 2023; revised 18 September 2023; accepted 21 September 2023; published 3 October 2023)

Low temperature, high resolution angle resolved photoemission experiments performed on bulk $1T$-$TiSe_2$ samples display conspicuous band folding as the only prominent signature of the periodic lattice distortion. The presence of a bulk electronic gap supporting a charge density wave phase is not confirmed in light of the new data. These observations cast serious doubts on the common belief of an electronic instability as the likely origin for the observed structural transition in $TiSe_2$.

DOI: 10.1103/PhysRevB.108.155105

I. INTRODUCTION

The large class and quasi-two-dimensional nature of transition metal dichalcogenides (TMDCs) provide fecund opportunities for studying various quantum states of matter [1–3]. In this connection, charge density wave (CDW) phases are notable as possible competitors to superconductivity and long-range ferromagnetic order [4,5]. Among the many TMDCs, $TiSe_2$ has long been under intense scrutiny. It undergoes a structural transition at ∼202 K with the formation of a $2a \times 2a \times 2c$ periodic lattice distortion [6,7]. This phenomenon is commonly attributed to a CDW transition and various models have been proposed to describe the underlying microscopic mechanism: (i) Fermi surface nesting [8], (ii) emergent antiferroelectric order [9], (iii) excitonic state [10–12], (iv) Jahn-Teller mechanism [13], and (v) combined electron-hole coupling and Jahn-Teller effect [14].

The common feature of all these models is the opening or modification of a bulk band gap between the Ti $3d$ conduction band (CB) and the Se $3p$ valence band (VB). In principle, the determination of such a gap should be straightforward for angle resolved photoemission (ARPES); in practice, evidences are ambiguous and lead to a profusion of models, each only partially supported by experimental data [12,15–17].

$TiSe_2$ is a particularly troubling case in that even the order of magnitude of the principal parameter in the models—the gap separating valence and conduction electrons in the distorted phase—is not established, with values ranging from 15 to 150 meV in the literature [17–22]. Not surprisingly, the experimental dispersion of the conduction band is also inconsistent. One set of studies reports a nearly flat CB located at the Fermi level [12,15–17], while a V-shaped CB extending about 100 meV below the Fermi level can be seen in other studies [18–20,23,24]. Intermediate CBs, with broader features, can also be found and are probably due to simultaneous probing of both bands [22,25,26]. An analogous situation is found for the valence band and particularly for an alleged backbending of the VB, usually interpreted as firm evidence of the presence of excitonic states presiding upon the structural phase transition [12,15–17,22].

At variance with the band structure studies, however, resistivity measurements do not show a prominent change across the structural transition at 202 K [27–29]. Furthermore, based on transport and optical measurements, $TiSe_2$ is a semimetal in the distorted phase [30,31]. This evidence apparently contradicts the computed and measured band structures, both claiming an emergent bulk band gap.

As a matter of fact the situation in $TiSe_2$ is complex. The periodic lattice distortion induces a conspicuous band folding in this material, forcing multiple bands in a narrow energy range [32–34]. And although the electronic structures of TMDCs are quasi-two-dimensional, each state displays strong spectral intensity variations with photon energy and/or experimental geometry. We believe that this photoemission cross-section effect is the major source of the present inconsistencies. It is interesting to notice that, considering all previous experimental results lumped together, a natural conclusion is a gapless band structure for bulk $1T$-$TiSe_2$ in the distorted phase, in open conflict with the majority of the proposed theoretical scenarios.

Here, we reexamine the electronic structure of bulk $1T$-$TiSe_2$ through extensive high-resolution ARPES measurements. Strictly adhering to the principle of only one reality, earlier experimental ARPES results and analysis are closely reproduced and extended with new ones, combining an attentive use of variable light polarization and experimental geometry. The overall picture that emerges for $TiSe_2$ in the distorted phase is of a metallic material without any bulk band gap separating the VB from the CB. Although these observations do not support the presence of CDW or excitonic insulator phases in this material, they clarify long-standing inconsistencies between ARPES data and are in good agreement with transport observations.

II. EXPERIMENTAL RESULTS AND DISCUSSION

Single crystal $1T$-$TiSe_2$ samples were grown through the floating zone method. The ARPES experiments were performed at the 21ID-I ESM beamline at the National Synchrotron Light Source II (NSLS-II), using a DA30 Scienta

*trgt2112@gmail.com

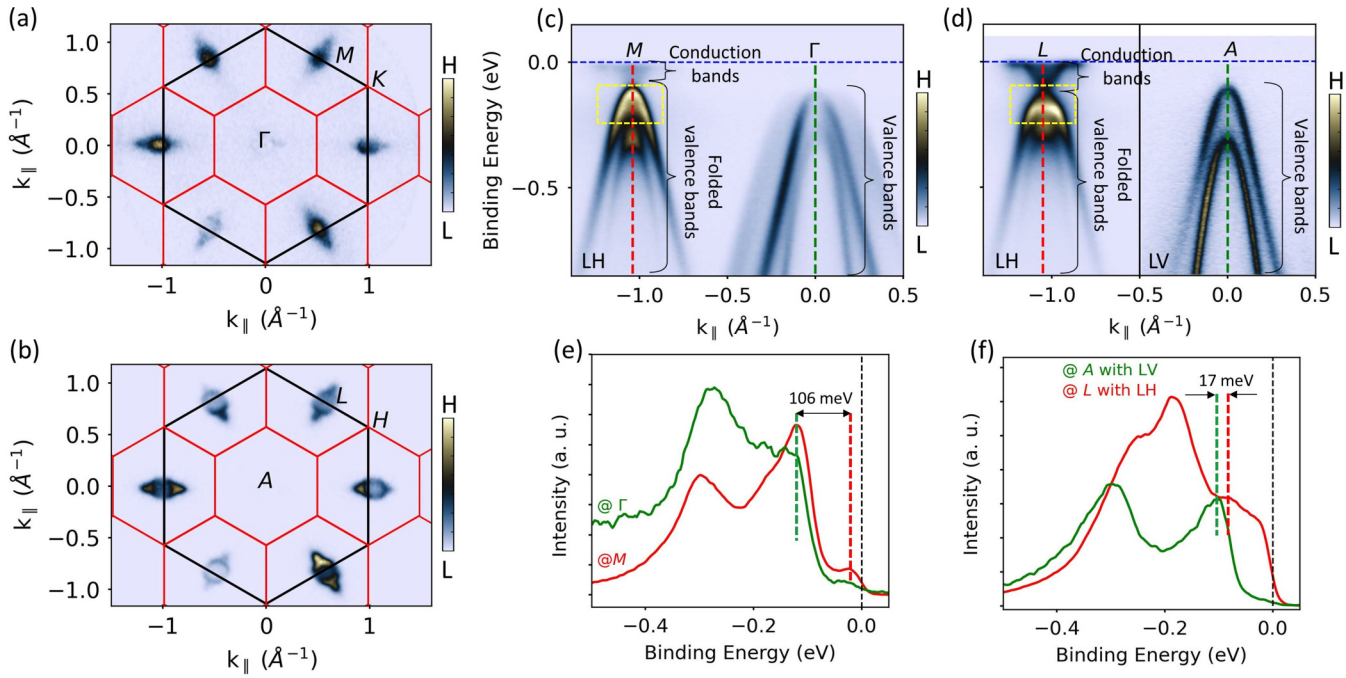

FIG. 1. (a), (b) Experimental Fermi surfaces for $1T$-$TiSe_2$ in the distorted phase at $\Gamma(h\nu = 99$ eV) and $A(h\nu = 119$ eV), respectively. (c), (d) ARPES spectra along the M-Γ-M and L-A-L directions. (e), (f) EDCs along the red and green dashed lines in (c) and (d). Vertical dashed green and red lines mark the probable bulk band gap as assigned in earlier reports. All spectra were measured with LH polarization except for the left panel in (d). Black and red hexagons in (a) and (b) represent the Brillouin zones of the normal and distorted phase, respectively. See the text for yellow dashed rectangles. The Fermi levels are also indicated in panels [(c)–(f)]. All the data are recorded at 15 K.

electron spectrometer with an energy resolution better than 15 meV. Samples were cooled by a closed-cycle He cryostat and cleaved at 15 K just before collecting the photoemission data. The synchrotron radiation incidence angle was 55°. The analyzer slit was along the $\overline{M}$-$\overline{\Gamma}$-$\overline{M}$ direction of the hexagonal Brillouin zone during the ARPES measurements at normal emission. The electric field of the linear vertical (LV) polarized light was parallel to the sample surface and analyzer slit while it was on the incident plane for linear horizontal (LH) polarized light.

The basic ARPES spectra for $TiSe_2$ in the distorted phase are reproduced in Fig. 1. These data are in excellent agreement with the one reported in the literature and display the main features used in the various models mentioned above. The principal Fermi surface sections at $k_z = \Gamma$ and A consist of circular features located at the high-symmetry points $M(L)$ of the hexagonal Brillouin zone and are decorated by small tails aligned along the $\Gamma(A)$-$M(L)$ direction [Figs. 1(a) and 1(b)]. The hallmark of the $2a \times 2a \times 2c$ periodic lattice distortion is the folding of the Se $4p$-derived VBs from Γ onto $M(L)$ [Figs, 1(c) and 1(d)]. Similarly, CB at the $M(L)$ point is expected to be folded onto the $\Gamma(A)$. However, due to the low spectral intensity, this part of the band structure appears as a faint feature that will be addressed later in this work. A gap between the VB at $\Gamma(A)$ and the CB at $M(L)$ points can be deduced from the energy distribution curves (EDCs) by identifiying the relative maxima with the band positions [see Figs. 1(e) and 1(f)]. This procedure yields gaps of 106 meV and 17 meV at k_z corresponding to the Γ plane and A plane, respectively. Both measured gaps have excellent correspondence in the literature [18,22]. However, they are not reliable measurements for the following reasons. First, CB bottom and VB top are not well defined at the Γ plane. Second, a high density of states is always present in the presumably gapped region. Third, the individual components are not resolved in the yellow dashed rectangular area where multiple bands coexist [Fig. 1(c)]. The same issues can be found in the earlier reports and are not unique to our case.

Furthermore, it is important to emphasize that the CB appearance changes dramatically with the photon energy. It has a V shape with a high density of state at the L point but a much weaker spectral intensity at the M point. Considering the highly two-dimensional nature of the material, this behavior is likely due to the variability of photoemission cross sections and cannot be attributed to intrinsic electronic band dispersion. Therefore, it is difficult to identify 2D and 3D bands to associate with an orbital selective gap opening.

On the other side, by expanding the investigation on higher-order zones and/or using different light polarization, it may be possible to exploit the matrix element effects to distinguish individual electronic states. These data are presented in Fig. 2. The Fermi energy cuts around six equivalent L points display very similar features, except for slight variations in the spectral intensity [Fig. 2(a)]. The corresponding binding energy versus $k_\parallel$ maps along the A-L-A direction are presented in Fig. 2(b) and probe the electronic structure in the region where the gap is expected to emerge. Clearly no empty region separates the conduction from the valence band. On the contrary, particularly cuts 2, 3, and 6 show a clear overlap between the CB and VB at ∼100 meV binding

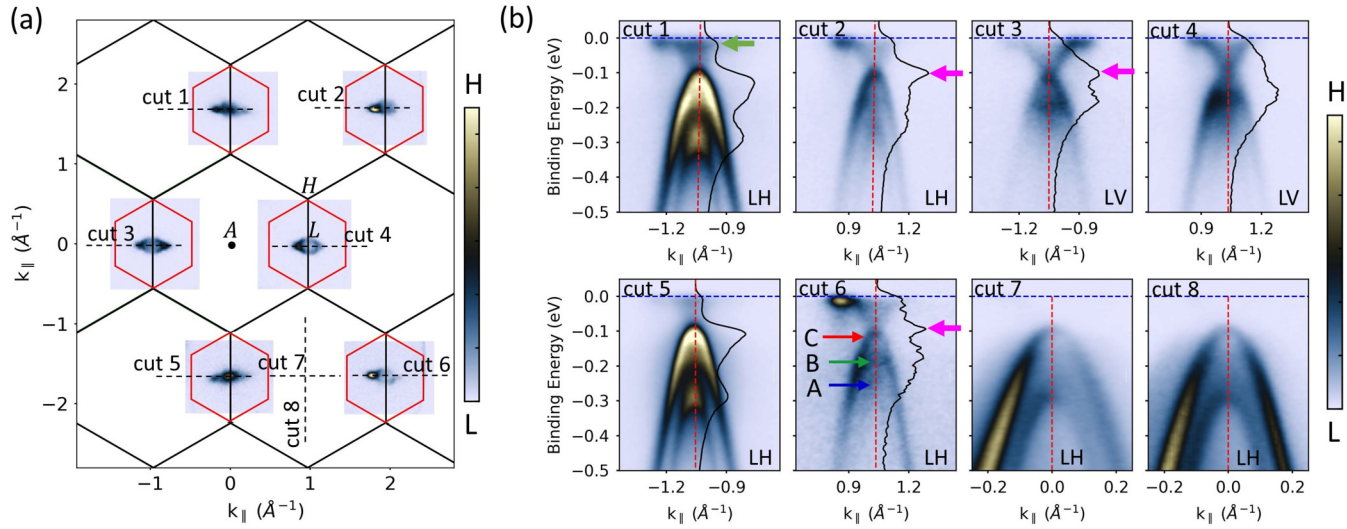

FIG. 2. (a) Multizone Fermi surfaces around six equivalent L points. LH polarization is used for these spectra. (b) Binding energy versus in-plane momentum maps along the corresponding dashed lines in (a). Cuts 1–7 are along the A-L direction while cut 8 is along the H-L direction. Photon polarization is given at the bottom of each spectrum. Pink arrows pointing at peaks in the EDCs signal overlaps between valence and conduction bands. All the data are collected with 119 eV lights at 15 K. Red, green, and blue horizontal arrows in cut 6 indicate the three components of the VB.

energy, highlighted by sharp peaks in the corresponding EDCs [see pink arrows in Fig. 2(b)]. The apparent bulk band gap extracted from cuts 1, 4, and 5 are clearly artifacts since all cuts represent the same band structure. Thereby, the surface electronic structure in the distorted phase is a semimetal in contrast to the general belief. It is also worth mentioning that the k_z will be slightly different at the higher Brillouin zones. But, this will have negligible impact on the conclusion due to the two-dimensional surface electronic structure that will be discussed in Fig. 4.

Furthermore, in the CB region, a relatively flat band located in the vicinity of the Fermi level is resolved in addition to the V-shaped one (marked with a green arrow in cut 1). A similar band can be found in previous studies and is usually attributed to backbending of the CB due to the formation of an excitonic insulator phase. However, the simultaneous observation of the V-shaped band makes these claims quite doubtful. The VB tip also does not exhibit a backbending at the A point as seen in the spectra taken along cuts 7 and 8, further opposing the hypothesis of an excitonic insulator state in $TiSe_2$.

It is also essential to reveal the gapless nature of the band structure in the zone center for the distorted phase. Figures 3(a) and 3(b) present the ARPES maps along the $\overline{K}$-$\overline{\Gamma}$-$\overline{K}$ and $\overline{M}$-$\overline{\Gamma}$-$\overline{M}$ directions, respectively. A weak V-shape

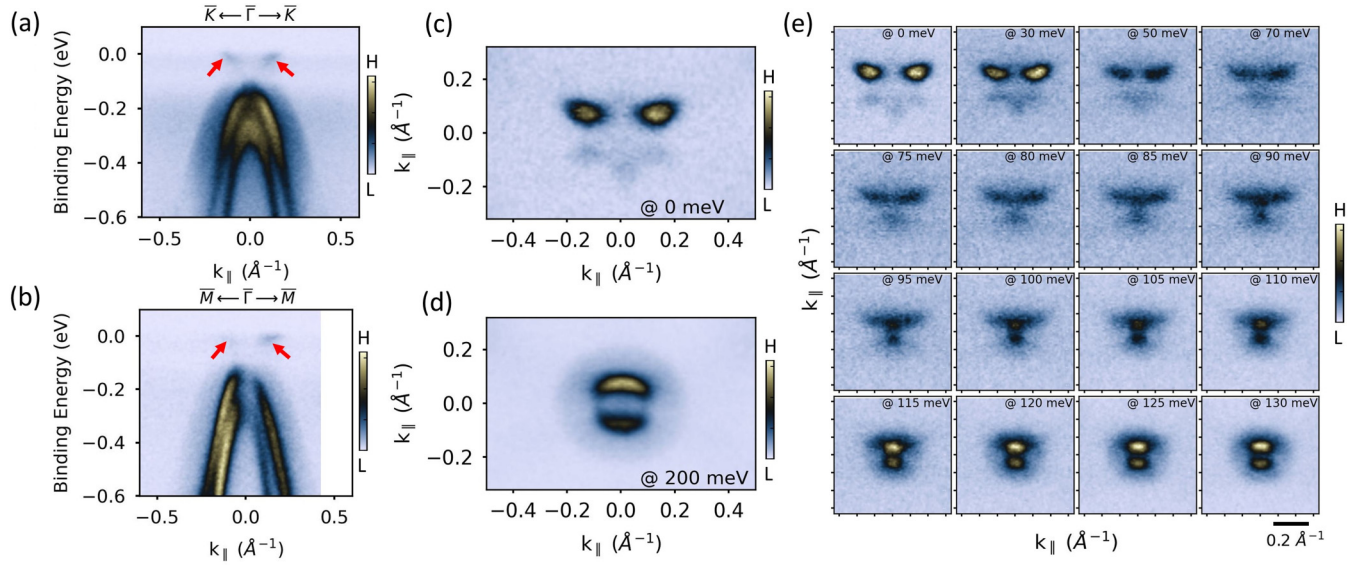

FIG. 3. (a), (b) ARPES maps along the $\overline{K}$-$\overline{\Gamma}$-$\overline{K}$ and $\overline{M}$-$\overline{\Gamma}$-$\overline{M}$ directions. (c), (d) Constant energy cuts at the Fermi level and at 200 meV below the Fermi level. (e) Constant energy cuts at various binding energies allow one to trace the gapless bulk band structure in the zone center. All the data were collected with 65 eV, LH polarized light, and at 15 K.

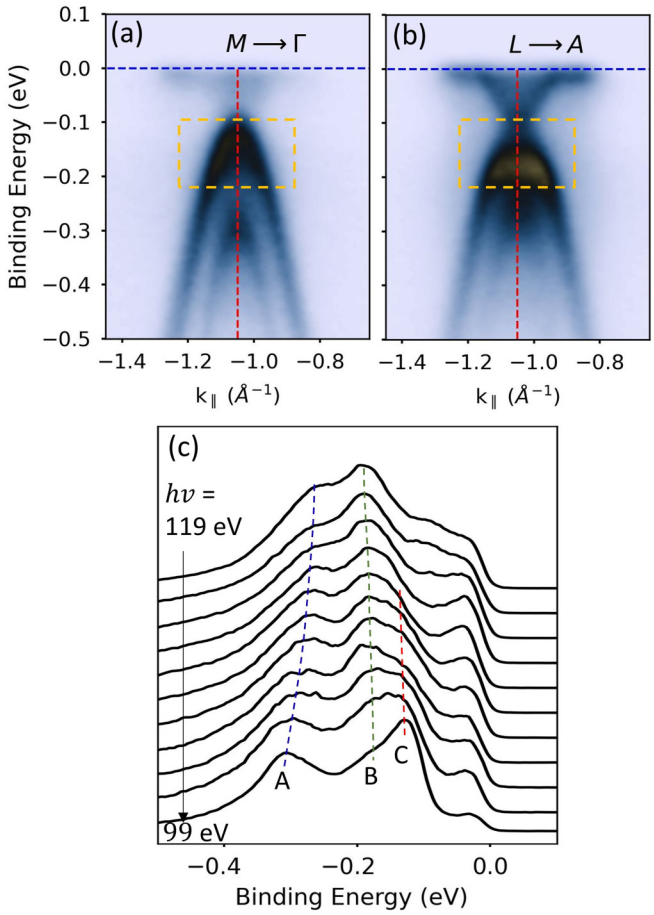

FIG. 4. (a), (b) ARPES spectra at M and L points, respectively. (c) EDCs along the $\overline{M}$ as a function of photon energy. Blue, green, and red dashed lines mark banding energies of the A, B, and C bands, respectively. Spectra are recorded at normal emission with LH polarized lights with 2 eV steps. 99 eV and 119 eV photon energies correspond to the $k_z = \Gamma$ and A high symmetry points, respectively. See the text for yellow dashed rectangles.

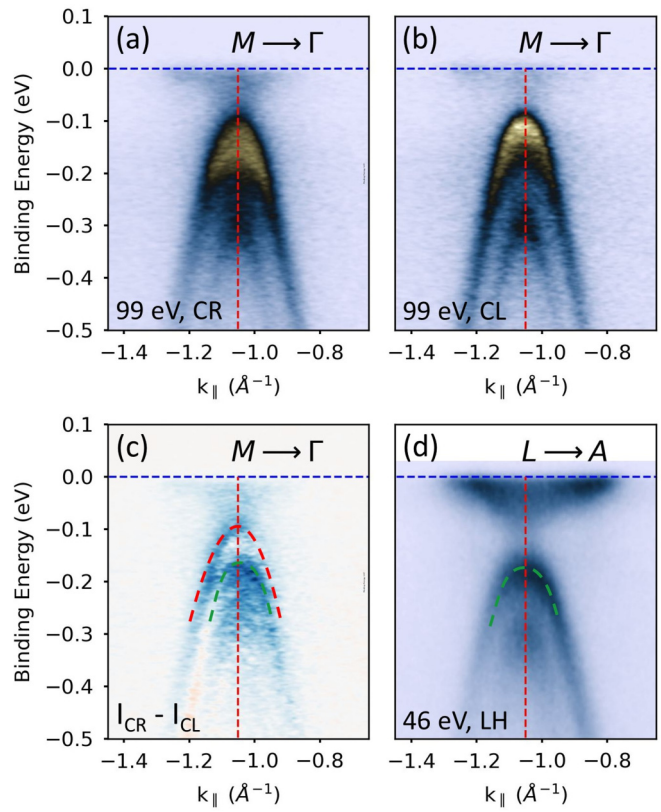

FIG. 5. (a), (b) ARPES spectra taken at M point with circular right (CR) and circular left (CL) light polarization. (c) Difference spectrum: (a), (b). (d) ARPES spectra taken with 46 eV corresponding to k_z at the L point and with LH polarized light. Green and red dashed lines highlight the B and C bands.

CB marked with red arrows can be seen in both spectra. The corresponding constant energy cuts evolves from a petal-like structure at the Fermi level [Fig. 3(c)] to a pair of momentum arcs surrounded by a circular halo in the CB region [Fig. 3(d)]. The detailed evolution with binding energy is shown in the panels of Fig. 3(e). As already observed at L, also at Γ, the electronic structure exhibits a continuum of states across the entire binding energy region of the alleged bulk band gap. Therefore, neither a direct nor an indirect bulk band gap is observed in the band structure of the periodically distorted $TiSe_2$ and the system is a semimetal.

Another scenario sometimes invoked to explain the structural transition in $1T$-$TiSe_2$ is the one of the excitonic insulator state. In this case, at low temperature, a k_z-dependent hybridization is assumed to take place between the folded CB and VB, resulting in a larger gap at the L point and a smaller one at the M point, due to dispersion of the VB. The experimental observations supporting this model are an energy shift and a flattening of the CB at the L point relative to the M point. However, the evidence presented in the literature is far from compelling [12,15–17].

An example of data leading to such an interpretation is given in Fig. 4. For consistency with the literature, the spectra are measured at normal emission with LH polarized light. The ARPES spectra at M and L points are presented side by side to facilitate the visualization of the energy shift and visual flattening of the VB [see yellow dashed rectangles in Figs. 4(a) and 4(b)]. Although these data are in line with previous observations, a closer look at the EDCs along the entire M-L high-symmetry line suggests a different origin for the apparent evolution of the CB with k_z [Fig. 4(c)]. Two distinct structures, B and C, are present in the binding energy region subtended by the yellow rectangles. Both features are present at all photon energies and, in agreement with the 2D nature of this material, display only moderate dispersion. It is only the relative variation of their spectral weights that gives the false impression of a binding energy shift, interpreted as a band backbending.

The absence of backbending in the bands at the M or L point is further confirmed using circularly polarized light and low photon energies (Fig. 5). At the M point (99 eV photon energy), the individual B and C components are clearly resolved in the circular dichroism spectrum [panel (c)] and do not display any sign of backbending flattening. Furthermore, probing the L point with lower photon energy [panel (d), 46 eV photon energy] enhances the dominating character of the B bands which also display a round top.

III. CONCLUSIONS

In summary, the bulk band structure of $TiSe_2$ does not host a direct or an indirect bulk band gap in the low T, distorted phase. This evidence is in sharp contrast with the majority of models currently used to describe the $2a \times 2a \times 2c$ structural phase transition. Earlier ARPES results have been reproduced and their interpretation has been shown to stem from poorly defined CB and VB edges. Backbending of the bulk bands as the origin of the indirect bulk band gap is also absent. The only prominent impact of the periodic lattice distortion is found to be the band folding due to the $2a \times 2a \times 2c$ superstructure. Additionally, our data also resolves the inconsistent electronic structures reported in the literature by constructing a more complete experimental band structure resulting from the observation of V-shaped and relatively flat components of the CB, simultaneously.

The overall findings presented here support the important conclusion that there is a critical mismatch between the theoretical and experimental band structures. Although both appear to be consistent in the literature, details of the band structure prove otherwise. We recently found similar issues in VSe_2 in which the surface electronic structure hosts multiple bands, not captured by the density functional theory [35]. Previous observation attributed the CDW phase in VSe_2 can be explained by using these data and shown to be not correlated with a pseudogap or Fermi surface nesting. Therefore, our results are likely to be generally applicable to other TMDCs, making the claims of CDW phases in these materials highly questionable.

ACKNOWLEDGMENTS

This research used resources ESM (21ID-I) beamline of the National Synchrotron Light Source II, a U.S. Department of Energy (DOE) Office of Science User Facility operated for the DOE Office of Science by Brookhaven National Laboratory under Contract No. DE-SC0012704.

We have no conflict of interest, financial or other, to declare.

[1] W. Choi, N. Choudhary, G. H. Han, J. Park, D. Akinwande, and Y. H. Lee, Recent development of two-dimensional transition metal dichalcogenides and their applications, Mater. Today **20**, 116 (2017).

[2] A. V. Kolobov and J. Tominaga, *Two-Dimensional Transition-Metal Dichalcogenides* (Springer, New York, 2016), Vol. 239.

[3] S. Manzeli, D. Ovchinnikov, D. Pasquier, O. V. Yazyev, and A. Kis, 2d transition metal dichalcogenides, Nat. Rev. Mater. **2**, 1 (2017).

[4] A. CastroNeto, Charge density wave, superconductivity, and anomalous metallic behavior in 2D transition metal dichalcogenides, Phys. Rev. Lett. **86**, 4382 (2001).

[5] K. Rossnagel, On the origin of charge-density waves in select layered transition-metal dichalcogenides, J. Phys.: Condens. Matter **23**, 213001 (2011).

[6] F. J. Di Salvo, D. Moncton, and J. Waszczak, Electronic properties and superlattice formation in the semimetal $TiSe_2$, Phys. Rev. B **14**, 4321 (1976).

[7] R. Craven, F. Di Salvo, and F. Hsu, Mechanisms for the 200 k transition in $TiSe_2$: A measurement of the specific heat, Solid State Commun. **25**, 39 (1978).

[8] A. Zunger and A. J. Freeman, Band structure and lattice instability of $TiSe_2$, Phys. Rev. B **17**, 1839 (1978).

[9] R. White and G. Lucovsky, Suppression of antiferroelectricity in $TiSe_2$ by excess carriers, Nuovo Cimento B **38**, 280 (1977).

[10] J. A. Wilson, Concerning the semimetallic characters of TiS_2 and $TiSe_2$, Solid State Commun. **22**, 551 (1977).

[11] J. A. Wilson, Modelling the contrasting semimetallic characters of TiS_2 and $TiSe_2$, Phys. Status Solidi B **86**, 11 (1978).

[12] T. Pillo, J. Hayoz, H. Berger, F. Lévy, L. Schlapbach, and P. Aebi, Photoemission of bands above the fermi level: The excitonic insulator phase transition in $1T$-$TiSe_2$, Phys. Rev. B **61**, 16213 (2000).

[13] H. P. Hughes, Structural distortion in $TiSe_2$ and related materials-a possible jahn-teller effect? J. Phys. C **10**, L319 (1977).

[14] J. van Wezel, P. Nahai-Williamson, and S. S. Saxena, Exciton-phonon-driven charge density wave in $TiSe_2$, Phys. Rev. B **81**, 165109 (2010).

[15] T. E. Kidd, T. Miller, M. Y. Chou, and T.-C. Chiang, Electron-hole coupling and the charge density wave transition in $TiSe_2$, Phys. Rev. Lett. **88**, 226402 (2002).

[16] H. Cercellier, C. Monney, F. Clerc, C. Battaglia, L. Despont, M. G. Garnier, H. Beck, P. Aebi, L. Patthey, H. Berger *et al.*, Evidence for an excitonic insulator phase in $1T$-$TiSe_2$, Phys. Rev. Lett. **99**, 146403 (2007).

[17] K. Rossnagel, L. Kipp, and M. Skibowski, Charge-density-wave phase transition in $1T$-$TiSe_2$: Excitonic insulator versus band-type Jahn-Teller mechanism, Phys. Rev. B **65**, 235101 (2002).

[18] M. D. Watson, O. J. Clark, F. Mazzola, I. Marković, V. Sunko, T. K. Kim, K. Rossnagel, and P. D. C. King, Orbital-and k_Z-selective hybridization of Se $4p$ and Ti $3d$ states in the charge density wave phase of $TiSe_2$, Phys. Rev. Lett. **122**, 076404 (2019).

[19] C. Monney, E. F. Schwier, M. G. Garnier, N. Mariotti, C. Didiot, H. Beck, P. Aebi, H. Cercellier, J. Marcus, C. Battaglia *et al.*, Temperature-dependent photoemission on $1T$-$TiSe_2$: Interpretation within the exciton condensate phase model, Phys. Rev. B **81**, 155104 (2010).

[20] A. Ghafari, L. Petaccia, and C. Janowitz, Splitting of the ti-3d bands of $TiSe_2$ in the charge-density wave phase, Appl. Surf. Sci. **396**, 1649 (2017).

[21] P. Chen, Y.-H. Chan, M.-H. Wong, X.-Y. Fang, M.-Y. Chou, S.-K. Mo, Z. Hussain, A.-V. Fedorov, and T.-C. Chiang, Dimensional effects on the charge density waves in ultrathin films of $TiSe_2$, Nano Lett. **16**, 6331 (2016).

[22] P. Chen, Y.-H. Chan, X.-Y. Fang, S.-K. Mo, Z. Hussain, A.-V. Fedorov, M. Chou, and T.-C. Chiang, Hidden order and dimensional crossover of the charge density waves in $TiSe_2$, Sci. Rep. **6**, 37910 (2016).

[23] J. Zhao, K. Lee, J. Li, D. B. Lioi, G. Karapetrov, N. Trivedi, and U. Chatterjee, Spectroscopic fingerprints of

many-body renormalization in $1T$-$TiSe_2$, Phys. Rev. B **100**, 045106 (2019).

[24] A. Wegner, J. Zhao, J. Li, J. Yang, A. A. Anikin, G. Karapetrov, K. Esfarjani, D. Louca, and U. Chatterjee, Evidence for pseudo–Jahn-Teller distortions in the charge density wave phase of $1T$-$TiSe_2$, Phys. Rev. B **101**, 195145 (2020).

[25] M. L. Adam, H. Zhu, Z. Liu, S. Cui, P. Zhang, Y. Liu, G. Zhang, X. Wu, Z. Sun, and L. Song, Charge density wave phase suppression in $1T$-$TiSe_2$ through Sn intercalation, Nano Res. **15**, 2643 (2022).

[26] C. Lian, S.-J. Zhang, S.-Q. Hu, M.-X. Guan, and S. Meng, Ultrafast charge ordering by self-amplified exciton–phonon dynamics in $TiSe_2$, Nat. Commun. **11**, 43 (2020).

[27] F. J. Di Salvo and J. V. Waszczak, Transport properties and the phase transition in $Ti_{1-x}M_xSe_2$(M = Ta or V), Phys. Rev. B **17**, 3801 (1978).

[28] I. Taguchi, M. Asai, Y. Watanabe, and M. Oka, Transport properties of iodine-free $TiSe_2$, Physica B+C **105**, 146 (1981).

[29] S. H. Huang, G. J. Shu, W. W. Pai, H. L. Liu, and F. C. Chou, Tunable Se vacancy defects and the unconventional charge density wave in $1T$-$TiSe_2$-δ, Phys. Rev. B **95**, 045310 (2017).

[30] K. Lee, J. Choe, D. Iaia, J. Li, J. Zhao, M. Shi, J. Ma, M. Yao, Z. Wang, C.-L. Huang *et al.*, Metal-to-insulator transition in Pt-doped $TiSe_2$ driven by emergent network of narrow transport channels, npj Quantum Mater. **6**, 8 (2021).

[31] G. Li, W. Z. Hu, D. Qian, D. Hsieh, M. Z. Hasan, E. Morosan, R. J. Cava, and N. L. Wang, Semimetal-to-semimetal charge density wave transition in $1T$-$TiSe_2$, Phys. Rev. Lett. **99**, 027404 (2007).

[32] T. Jaouen, B. Hildebrand, M.-L. Mottas, M. Di Giovannantonio, P. Ruffieux, M. Rumo, C. W. Nicholson, E. Razzoli, C. Barreteau, A. Ubaldini *et al.*, Phase separation in the vicinity of fermi surface hot spots, Phys. Rev. B **100**, 075152 (2019).

[33] R. Bianco, M. Calandra, and F. Mauri, Electronic and vibrational properties of $TiSe_2$ in the charge-density-wave phase from first principles, Phys. Rev. B **92**, 094107 (2015).

[34] S.-M. Huang, S.-Y. Xu, B. Singh, M.-C. Hsu, C.-H. Hsu, C. Su, A. Bansil, and H. Lin, Aspects of symmetry and topology in the charge density wave phase of $1T$-$TiSe_2$, New J. Phys. **23**, 083037 (2021).

[35] T. Yilmaz, E. Vescovo, and B. Sinkovic, Multiband Fermi surface in $1T$-$TiSe_2$ and its implication for the charge density wave phase, Phys. Rev. B **107**, 165109 (2023).